Applied Chemical Engineering (2026) Volume 9 Issue 2 ISSN: 2578-2010 (O)
doi: 10.59429/ace.v9i2.5970

RESEARCH ARTICLE

Process-Integrated Hydrogen Energy Storage, Carbon Capture, and PEV Coordination in Renewable-Assisted Power Systems: A Chemical Engineering Optimization Perspective

Abhilasha Pawar[1], Y V Krishna Reddy[2,*], Víctor Daniel Jiménez Macedo[3], Lizina Khatua[4], Feroz Shaik[5], Subhasis Datta[6], Kamalika Tiwari[6], C. KARNAN[7]

[1] *Department of Electrical Engineering, JSS Academy of Technical Education, Noida, 201301, India*
School of Engineering, Department of Electrical Engineering, JSS University, Noida(U.P),India
[2] *Department of EEE, SV College of Engineering, Tirupati, 517501, India*
[3] *Mechanical Engineer Faculty, Michoacan University of Saint Nicholas of Hidalgo, 78557, Hidalgo*
[4] *School of Electronics Engineering, Kalinga Institute of Industrial Technology(KIIT) Deemed to be University, Bhubaneswar, Odisha, 751024, India*
[5] *Department of Mechanical Engineering, Prince Mohammad Bin Fahd University, Alkhobar, 34411, Kingdom of Saudi Arabia*
[6] *Dr. B. C. Roy Engineering College, Durgapur, West Bengal, 713206, India*
[7] *Dapartment of Mathmatics, K. Ramakrishnan College of Engineering, Samayapuram, Trichy,621112, India*
***Corresponding author:** Y V Krishna Reddy, yvkrishnareddy36@gmail.com

ABSTRACT

This study presents a process-integrated framework for hydrogen energy storage and post-combustion carbon capture within renewable-assisted power systems, explicitly incorporating plug-in electric vehicle (PEV) interactions. In contrast to conventional economic load dispatch (ELD) formulations that treat hydrogen and carbon capture as simplified energy components, the proposed approach adopts a process-oriented representation of electrolyzer-based hydrogen production, fuel cell energy conversion, and amine-based CO_2 absorption. The framework captures the coupling between electrical energy flows and chemical processes through energy–mass balance relationships and efficiency constraints. PEVs are modelled as flexible electrochemical storage systems with bidirectional vehicle-to-grid (V2G) capability, enabling dynamic interaction with system demand. The integrated model is formulated as a multi-objective optimization problem, considering operating cost and emission reduction, and is solved using the Zebra Optimization Algorithm (ZOA). The framework is evaluated on a standard ten-unit test system under multiple operational scenarios. Results indicate that renewable and PEV integration reduces emissions by 19% and operating cost by 10%. The inclusion of hydrogen energy storage and 90% efficient carbon capture achieves approximately 80% emission reduction with a moderate increase in cost. These findings highlight the significance of incorporating process-level chemical engineering principles into power system optimization, demonstrating that coordinated hydrogen production, utilization, and carbon capture can substantially enhance decarbonization performance while maintaining system feasibility.

ARTICLE INFO

Received: 02 April 2026
Accepted: 28 May 2026
Available online: 12 June 2026

Keywords: Hydrogen energy storage, Carbon capture and storage, Process-integrated energy systems, Plug-in electric vehicles, Multi-objective optimization, Renewable-assisted power systems

Nomenclature

Symbol	Description	Unit
F_{Total}	Total operating cost of the system	$
$F_{Thermal}$	Cost of thermal power generation	$
F_{Wind}	Cost associated with wind power generation	$
F_{Solar}	Cost associated with solar power generation	$
F_{PEV}	Cost related to PEV charging/discharging operations	$
$F_{Hydrogen}$	Cost of hydrogen production and utilization	$
F_{CCS}	Cost of carbon capture and storage	$
$F_{Emission}$	Cost associated with emission penalties	$
a_i	No-load cost coefficient of generator i	$
b_i	Linear cost coefficient of generator i	$/MW
c_i	Quadratic cost coefficient of generator i	$/MW²
d_i	Valve-point loading coefficient	$
e_i	Valve-point frequency coefficient	1/MW
$P_{i,min}$	Minimum operating limit of generator i	MW
v	Wind speed	m/s
k	Shape parameter of Weibull distribution	–
c	Scale parameter of Weibull distribution	m/s
v_i	Cut-in wind speed	m/s
v_r	Rated wind speed	m/s
v_o	Cut-out wind speed	m/s
P_r	Rated power of wind turbine	MW
C_w	Direct wind generation cost coefficient	$/MW
C_{over}	Penalty cost for overestimation of wind power	$/MW
C_{under}	Penalty cost for underestimation of wind power	$/MW
$P_{sch,t}$	Scheduled wind power	MW
$P_{av,t}$	Available wind power	MW
d_s	Direct solar generation cost coefficient	$/MW
$k_{r,s}$	Penalty cost for overestimation of solar power	$/MW
$k_{p,s}$	Penalty cost for underestimation of solar power	$/MW
s_t	Scheduled solar power at time t	MW
s_{av}	Available solar power	MW
G	Solar irradiance	W/m²
G_{std}	Standard irradiance	W/m²
R_c	Reference irradiance threshold	W/m²
s	Solar power output factor	–
s_r	Rated solar power factor	–

f_G	Solar generation function coefficient	–
$H_{prod,t}$	Hydrogen produced by electrolyzer at time t	kg
$H_{use,t}$	Hydrogen consumed by fuel cell at time t	kg
H_{min} , H_{max}	Min and Max hydrogen storage limit	kg
$P_{PEV,t}$	Net PEV power at time t	MW
η_c	Charging efficiency of PEV battery	–
η_d	Discharging efficiency of PEV battery	–
SOC_{min} , SOC_{max}	Min, Max state of charge limit	–
η_{CCS}	Carbon capture efficiency	–
$CO_{2,captured,t}$	Amount of CO_2 captured at time t	kg
$CO_{2,net,t}$	Net CO_2 emissions after capture	kg
$CO_{2,thermal,t}$	CO_2 emissions from thermal generators	kg
C_{CCS}	Cost coefficient for carbon capture	$/kg

1. Introduction

In chemical engineering, the integration of hydrogen energy storage and carbon capture into modern power systems requires process-level modelling that is often overlooked in conventional dispatch formulations. Electrochemical kinetics, membrane ion transport, and temperature-dependent efficiencies govern hydrogen production through water electrolysis. Similarly, post-combustion carbon capture using amine absorption involves complex gas–liquid interactions, reaction equilibria, and energy-intensive solvent regeneration. These physicochemical processes significantly influence system efficiency, operational cost, and emission reduction performance. Therefore, incorporating such process-level behaviour is essential for realistic and meaningful techno-economic optimization. In this context, the present study develops a process-integrated framework that captures electrolyzer operation, fuel cell dynamics, and amine-based carbon capture within a renewable-assisted power system.

In contrast, most existing Economic Load Dispatch (ELD) and Dynamic Economic Emission Dispatch (DEED) models represent hydrogen and carbon capture subsystems using simplified input–output relationships. Although these simplified models reduce computational complexity, they fail to capture critical interactions between process performance and system-level decision-making. Consequently, there is a clear need to integrate chemical process modelling with power system optimization within a unified framework.

The increasing penetration of renewable energy sources (RES), together with the rapid adoption of plug-in electric vehicles (PEVs), has significantly transformed power system operation. What was previously a cost-oriented optimization problem has evolved into a nonlinear, multi-objective framework characterized by variability, uncertainty, and flexible demand. Renewable intermittency, bidirectional PEV charging and discharging, and the integration of low-carbon technologies such as hydrogen storage and carbon capture introduce additional operational challenges. These developments have driven the need for advanced optimization methods and integrated modelling approaches.

Earlier studies on ELD primarily focused on thermal generation systems. Optimization techniques such as Teaching–Learning-Based Optimization [1], Ant Lion Optimization [2], and Mountaineering Team-Based Optimization [3] were proposed to improve cost efficiency and constraint handling. However, these approaches did not consider renewable integration or emerging energy technologies. Subsequent research incorporated

renewable energy sources into dispatch models. Wind power uncertainty was analysed in [4], while broader renewable-integrated dispatch formulations were presented in [5] and [6]. Despite these advancements, the combined impact of PEVs, hydrogen systems, and carbon capture has not been fully addressed.

The integration of PEVs into dynamic dispatch frameworks has been widely investigated to enhance system flexibility and reduce emissions. Studies such as [7–10] explored coordinated wind–EV and solar–EV dispatch strategies, while [11–16] extended these models to include uncertainty and multi-objective optimization. Although these contributions demonstrate the advantages of PEV participation, they do not consider interactions with hydrogen-based energy storage and carbon capture technologies.

Parallel research has examined hydrogen energy systems and carbon capture integration. Reviews on hydrogen production and storage are provided in [22], while renewable-driven hydrogen generation is discussed in [23]. Multi-energy dispatch frameworks incorporating hydrogen and thermal systems are presented in [24] and[25], and carbon capture-based dispatch strategies are developed in [26] and [27]. However, these studies generally treat hydrogen and carbon capture independently and do not integrate them with PEV-supported renewable dispatch in a unified optimization framework.

Based on the literature [1–33], it is evident that most existing approaches address individual components of modern power systems in isolation. A comprehensive framework that simultaneously considers renewable-assisted dispatch, PEV participation with vehicle-to-grid capability, hydrogen energy storage via electrolyzer–fuel cell systems, and carbon capture with realistic efficiency constraints remains underdeveloped.

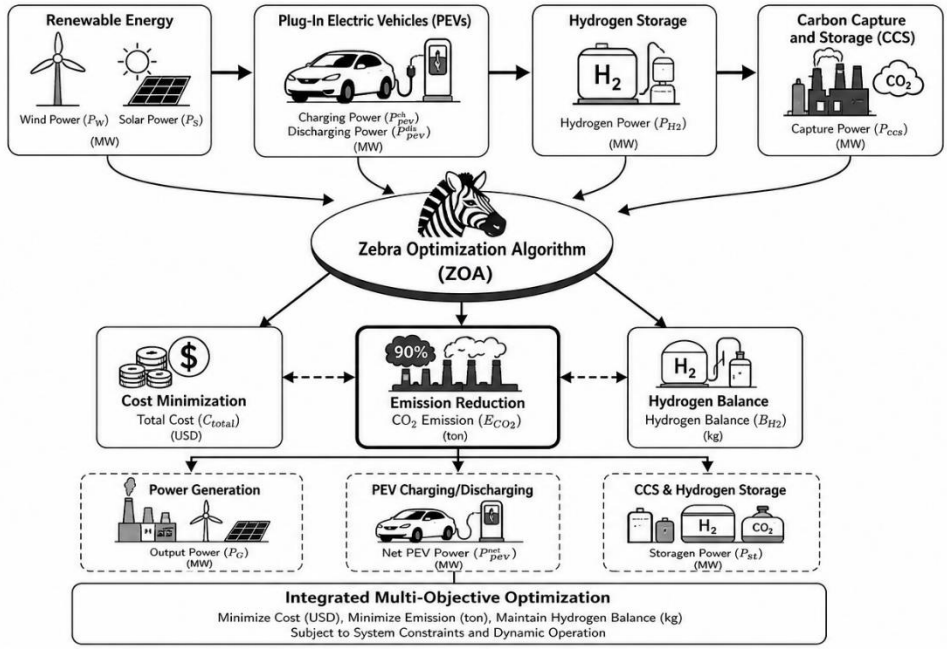

Figure 1. Hydrogen–CCS Integrated DEED Framework

To address these limitations, this study proposes a unified DEED framework that integrates RES, PEVs, hydrogen energy storage, and carbon capture into a single multi-objective optimization model. The Zebra Optimization Algorithm (ZOA) [33] is employed to solve the resulting nonlinear problem, ensuring stable convergence while maintaining hydrogen balance and emission reduction targets. The proposed framework provides a scalable and practically viable pathway for low-carbon power system operation, while explicitly linking chemical process behaviour with system-level optimization.

Figure 1 illustrates the proposed DEED framework integrating RES, PEVs, hydrogen energy storage, and CCS. The system is optimized using the ZOA to achieve coordinated cost minimization, emission reduction, and hydrogen energy balance.

2. Problem Formulation

This section presents the mathematical formulation of the proposed 24-hour Dynamic Economic Emission Dispatch (DEED) problem, incorporating thermal generating units, wind and solar renewable sources, plug-in electric vehicles (PEVs), hydrogen energy storage (electrolyzer–fuel cell system), and carbon capture and storage (CCS).

In contrast to conventional DEED models, the proposed formulation adopts process-informed representations of hydrogen production and carbon capture. The electrolyzer and fuel cell are modelled using energy–mass conversion relationships, while the CCS system incorporates capture efficiency and associated energy penalties to provide a realistic techno-economic representation. The objective is to minimize total operating cost and emissions subject to system equality and inequality constraints. The resulting nonlinear multi-objective problem is solved using the Zebra Optimization Algorithm (ZOA) [33]. All variables are defined in the Nomenclature section, and key governing equations are highlighted in bold for clarity.

2.1. Objective Functions

2.1.1. Total Generation Cost

The total 24-hour operating cost is expressed as Eqn. (1):

$$\mathbf{F_{Total} = F_{Thermal} + F_{Wind} + F_{Solar} + F_{PEV} + F_{Hydrogen} + F_{CCS} + F_{Emission}} \quad (1)$$

2.1.1.1. Thermal Generation Cost

For an N-unit system with valve-point effects expressed as Eqn. (2):

$$\mathbf{F_{Thermal} = \sum_{t=1}^{24}\sum_{i=1}^{N}[a_i + b_i P_{i,t} + c_i P_{i,t}^2 + |\, d_i \sin(e_i(P_{i,min} - P_{i,t}))|\,]} \quad (2)$$

Where a_i, b_i, c_i are quadratic/linear/no-load coefficients; e_i, f_i model valve-point loading discontinuities.

2.1.1.2. Wind Cost (Weibull-distributed availability):

Wind speed follows Weibull distribution expressed as Eqn. (3):

$$f(v) = \frac{k}{c}\left(\frac{v}{c}\right)^{k-1} e^{-(v/c)^k} \quad (3)$$

Wind turbine output expressed as Eqn. (4):

$$P_{wind,t} = \begin{cases} 0 & v_t < v_i \\ P_r \dfrac{(v_t - v_i)}{(v_r - v_i)} & v_i \le v_t < v_r \\ Pr & v_r \le v_t \le v_o \\ 0 & v_t > v_o \end{cases} \quad (4)$$

Total wind cost expressed as Eqn. (5):

$$F_{Wind} = \sum_{t=1}^{24}[C_w P_{wind,t} + C_{over}(P_{sch,t} - P_{av,t}) + C_{under}(P_{av,t} - P_{sch,t})] \quad (5)$$

- Direct cost: $C_w P_{wind,t}$
- Overestimation penalty: $C_{over} = \int_{v_t}^{0} (v_t - v\,) P_{wind,t} dv$ (6)
- Underestimation penalty: $C_{under} = \int_{v_r}^{v_t} (v\, - v_t) P_{wind,t} dv$ (7)

where $P_{wind,t}$ follows Weibull PDF with scale c_w, shape C_w, cut-in V_i, rated V_r

The wind farm delivers 175 MW of power using Weibull parameters (k = 1.5, c = 15 m/s) and turbine limits (v_i = 5 m/s, v_r = 15 m/s, v_o = 45 m/s) [12].

2.1.1.3. Solar Cost (Bimodal Weibull irradiation):

$$F_{solar}(S_t) = d_s s_t + k_{r,s}(s_t - s_{av}) + k_{p,s}(s_{av} - s_t) \quad (8)$$

Solar PDF combines two Weibull's based on irradiation G:

$$f_s(s) = \begin{cases} f_G\left(\frac{sG_{std}}{s_r R_c}\right) & G \geq R_c \\ \frac{1}{2}\sqrt{\frac{R_c G_{std}}{s_r}} s f_G\left(\sqrt{\frac{sR_c G_{std}}{s_r}}\right) & 0 \leq G < R_c \end{cases} \quad (9)$$

$G_{std} = 1000 W/m^2, R_c = 150 W/m^2$

Daily solar irradiance data with 175 MW rated PV capacity and ω = 0.3 uncertainty factor is employed to predict available and planned solar power using nonlinear and linear regions [12].

2.1.1.4. Plug-in Electric Vehicle Parameters

Net PEV power: $\mathbf{P_{PEV,t} = P_{charge,t} - P_{discharge,t}}$ (10)

SOC update: $SOC_{t+1} = SOC_t + \eta_c P_{charge,t} - \frac{P_{discharge,t}}{\eta_d}$ (11)

Subject to: $SOC_{min} \leq SOC_t \leq SOC_{max}$ (12)

One shipment day assessed 80,000 charging PEVs. Based on Table 1 PEV data, total charging capacity is determined as follows:

$$\begin{aligned} &\text{Total Charging Load} = 80000 * [0.3 * 40 * (0.8 - 0.3) \\ &+ (0.45 * 15 * (0.95 - 0.05) + 0.25 * 25 * (0.9 - 0.1)] / 1000 \\ &= 1366 \text{ MW} \end{aligned}$$

Table 1. Typical Parameters of PEV

Vehicle category	Share in fleet (%)	Battery energy (kWh)	Lower SOC limit (%)	Upper SOC limit (%)
Battery EVs	30	40	30	80
Mild hybrid EVs	45	15	5	95
Full hybrid EVs	25	25	10	90

The PEV parameters and fleet composition are selected based on standard datasets and typical vehicle specifications reported in recent literature [14], ensuring realistic modelling of charging demand and V2G operation. Vehicle-to-grid (V2G) support included 20,000 discharging PEVs and half the state-of-charge capacity. Total discharge power:

$$\begin{aligned} &\text{Total Discharging Load} = 20000 * [0.3 * 40 * (0.8 - 0.3) / 2 \\ &+ (0.45 * 15 * (0.95 - 0.05) / 2 + 0.25 * 25 * (0.9 - 0.1) / 2] / 1000 \\ &= 170.75 \text{ MW} \end{aligned}$$

2.1.2. Hydrogen Energy Storage Modelling

Hydrogen system includes electrolyzer and fuel cell. Unlike conventional simplified models, hydrogen storage is formulated using energy-to-mass conversion principles.

Electrolyzer power: $$\mathbf{P_{EL,t}} = \frac{\mathbf{H_{prod,t}}}{\boldsymbol{\eta}_{\mathbf{EL}}} \quad (13)$$

Fuel cell power: $$\mathbf{P_{FC,t}} = \boldsymbol{\eta}_{\mathbf{FC}} \mathbf{H_{use,t}} \quad (14)$$

Hydrogen storage balance: $$\mathbf{H_{t+1}} = \mathbf{H_t} + \mathbf{H_{prod,t}} - \mathbf{H_{use,t}} \quad (15)$$

Hydrogen limits: $$H_{min} \le H_t \le H_{max} \quad (16)$$

Hydrogen cost: $$F_{Hydrogen} = \sum_{t=1}^{24} (C_{EL} P_{EL,t} + C_{FC} P_{FC,t}) \quad (17)$$

2.1.3. Carbon Emission Model

Exponential and quadratic emission estimates for each generator environmental performance.

$$E_i(P_i) = \sum_{i=1}^{N} (\alpha_i P_i^2 + \beta_i P_i^2 + \gamma_i + \delta_i e^{\varepsilon_i P_i}) \quad (18)$$

Total emission: $$F_{Emission} = \sum_{t=1}^{24} \sum_{i=1}^{N} E_i(P_i) \quad (19)$$

where $\alpha_i, \beta_i, \gamma_i$ represent the emission coefficients and δ_i, ε_i scale the exponential emission component.

2.1.4. Carbon Capture and Storage (CCS)

Captured CO_2: $$\mathbf{CO_{2,captured,t}} = \boldsymbol{\eta}_{\mathbf{CCS}} \text{證} \ \mathbf{O_{2,thermal,t}} \quad (20)$$

Net emission: $$\mathbf{CO_{2,net,t}} = (\mathbf{1} - \boldsymbol{\eta}_{\mathbf{CCS}}) \mathbf{CO_{2,thermal,t}} \quad (21)$$

CCS cost: $$F_{CCS} = \sum_{t=1}^{24} C_{CCS} \cdot CO_{2,captured,t} \quad (22)$$

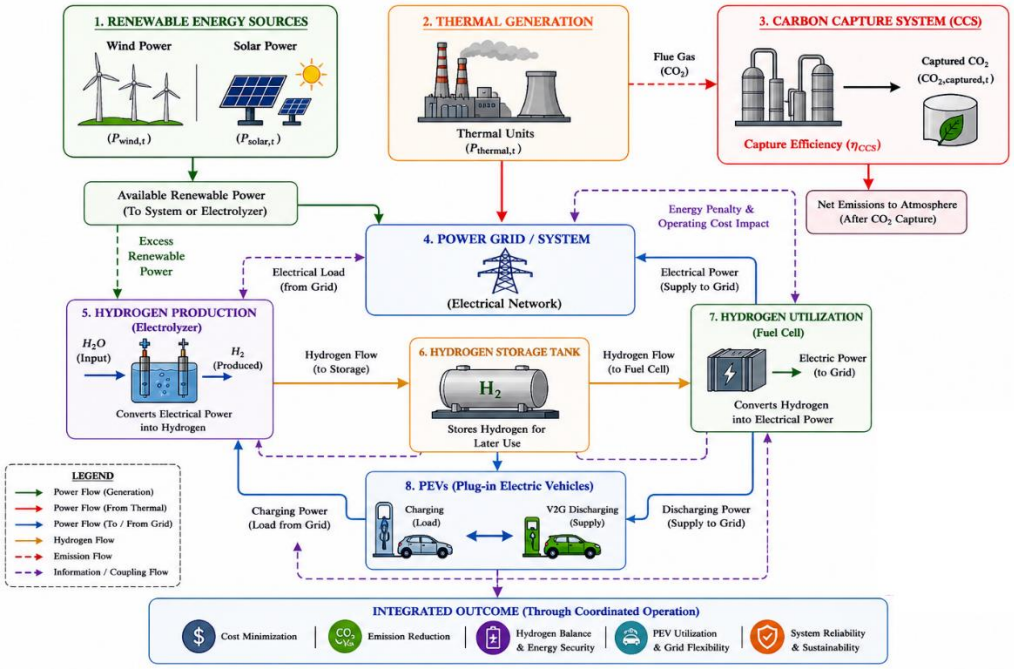

Figure 2. Integrated Multi-Energy Coupling of PEV, Hydrogen Storage, and CCS

Figure 2 illustrates the integrated multi-energy coupling among renewable sources, PEVs, hydrogen energy storage, and CCS within the proposed system. Renewable power is first utilized to meet grid demand, while surplus energy is directed to the electrolyzer for hydrogen production and stored for later use. The stored hydrogen is converted back into electricity through the fuel cell during peak demand periods, ensuring energy shifting and system flexibility. PEVs interact bidirectionally with the grid by charging during low-demand periods and supplying power during peak conditions through V2G operation. Thermal generation supports base load demand, and the associated CO_2 emissions are captured using the CCS system, thereby reducing net emissions. All these components are interconnected and coordinated through the system power balance, ensuring efficient, reliable, and environmentally sustainable operation.

2.1.5. Power Loss Calculation

Kron loss formula:

$$P_{loss,t} = P_g^{t} B P_g \tag{23}$$

where B is 10×10 symmetric loss coefficient matrix, $P_g = [P_{g1}, ..., P_{g10}, w_t, s_t]^T$

2.2. Constraints

2.2.1. Power Balance (Equality)

$$\sum P_{thermal,t} + P_{wind,t} + P_{solar,t} + P_{FC,t} + P_{discharge,t} = P_{Load,t} + P_{EL,t} + P_{charge,t} + P_L \tag{24}$$

2.2.2. Generator Limits (Inequality)

$$P_{gi,min} \le P_{gi,t} \le P_{gi,max}, i = 1, ..., N \tag{25}$$

2.2.3. Ramp Rate Limits

$$P_{gi,t-1} - DR_i \le P_{gi,t} \le P_{gi,t-1} + UR_i \tag{26}$$

2.2.4. Prohibited Operating Zones (POZ)

$$P_{gi,t} \notin (P_{i,Z}^L, P_{i,Z}^U), Z = 1, ..., Z_i \tag{27}$$

2.2.5. Spinning Reserve

$$\sum_{i=1}^{N} \min(P_{i,max} - P_{gi,t}, UR_i) + (w_r - w_t) + (s_r - s_t) \geq SR_t = \frac{P_{d,t} + P_{ch,t} - P_{disch,t}}{120} \quad (28)$$

2.3. Multi-Objective Fitness Function

The combined objective is transformed into a weighted penalty function:

$$\begin{aligned} \textbf{Fitness} = {} & \mathbf{w_1 F_{Total} + w_2 F_{Emission} + \lambda_1 (Power\ Balance\ Penalty)} \\ & \mathbf{+ \lambda_2 (Hydrogen\ Violation)} \end{aligned} \quad (29)$$

2.4. Solution Methodology

Due to valve-point nonlinearity, renewable generation uncertainty, hydrogen mass–energy coupling, and the inclusion of CCS energy penalties, the formulated problem becomes highly non-convex and multi-modal.

Therefore, the Zebra Optimization Algorithm (ZOA) [33] is employed to:

- Ensure global search capability
- Maintain exploration–exploitation balance
- Handle nonlinear constraints
- Achieve stable convergence

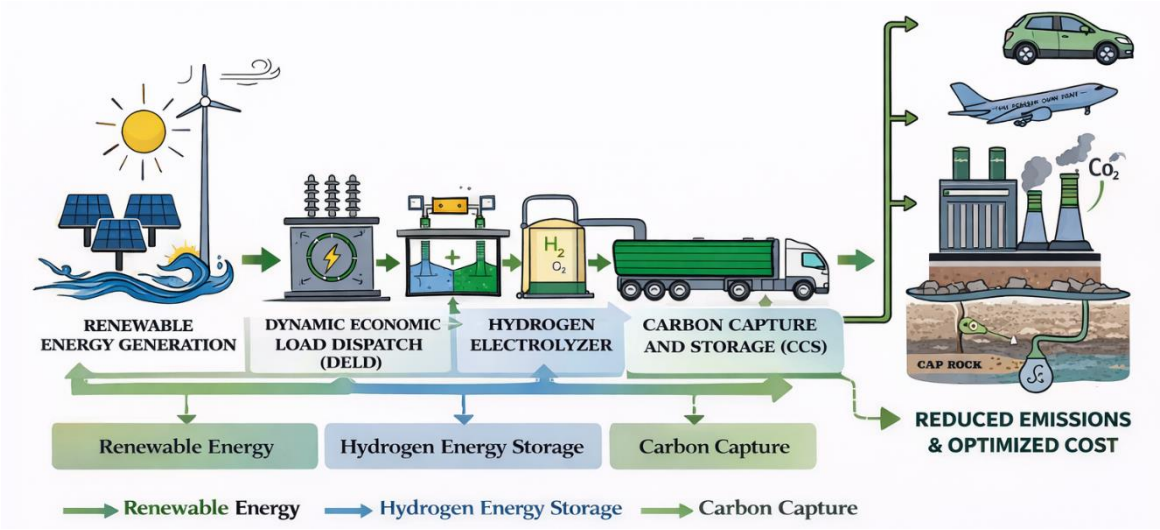

Figure 3. System Configuration for Hydrogen–CCS Integrated DELD Problem Formulation

Figure 3 presents the structural configuration used in the problem formulation, integrating renewable generation, hydrogen energy storage, and carbon capture within the DEED framework. It illustrates the energy flow pathways and emission control mechanisms incorporated into the 24-hour multi-objective optimization model.

3. Zebra Optimization Algorithm (ZOA)

The Dynamic Economic Emission Dispatch (DEED) problem formulated in this study is highly nonlinear and non-convex due to valve-point effects, renewable intermittency, hydrogen storage dynamics, carbon capture coupling, and transmission losses. These characteristics result in a complex multi-modal search space, making conventional gradient-based optimization techniques ineffective for obtaining global optimal solutions.

To address this challenge, the Zebra Optimization Algorithm (ZOA) [33] is employed. ZOA is a nature-inspired metaheuristic that mimics the social foraging and survival behaviour of zebra herds through three main phases:

1. Exploration Phase: a search around the whole solution space
2. Exploitation Phase—moving toward the best zebra that is the most common
3. Diversification Phase: a way to keep things from converging too soon

3.1. Population & Fitness Landscape

Search Space: N=50 zebras, $X_i(t) \in [0,1]$ (30)

Each zebra represents a candidate dispatch vector:

$$X_i = [x_{i1}, x_{i2}, ..., x_{iD}] \quad (31)$$

where D=12 corresponds to 10 thermal units, electrolyzer, and fuel cell variables.

Initial population is generated randomly within lower and upper bounds:

$$X_{i,j} = LB_j + rand(0,1)(UB_j - LB_j) \quad (32)$$

Fitness of each zebra is evaluated using the multi-objective function defined in Chapter 2.

3.2. Position Update Mechanism

At each iteration, the zebra with minimum fitness is selected as the alpha zebra:

$$X_\alpha = \text{argmin}Fitness(X_i) \quad (33)$$

Each zebra updates its position using one of the following three phases.

3.2.1. Exploration Phase

With 50% probability, global roaming behaviour is simulated:

$$X_i^{t+1} = X_i^t + r_1(X_\alpha - X_i^t) \quad (34)$$

where r_1 is a uniformly distributed random vector. This phase enhances global search capability and prevents early stagnation.

3.2.2. Exploitation Phase

To refine solutions near promising regions:

$$X_i^{t+1} = X_i^t + \alpha(X_\alpha - X_i^t) \quad (35)$$

where α is the exploitation factor. This stage accelerates convergence toward optimal dispatch values.

3.2.3. Diversification Phase

To avoid local optima trapping:

$$X_i^{t+1} = X_i^t + \beta \cdot randn(0,1) \quad (36)$$

where β is the diversification factor. This introduces controlled perturbation in the search process.

3.3. Selection Strategy

If the updated candidate improves the fitness:

$$Fitness(X_i^{new}) \leq Fitness(X_i^t) \quad (37)$$

then the new position is accepted; otherwise, the previous solution is retained.

3.4. Boundary Handling

All updated variables are maintained within permissible limits:

$$X_{i,j} = \min(\max(X_{i,j}, LB_j), UB_j) \tag{38}$$

This ensures feasibility of generator outputs and storage limits.

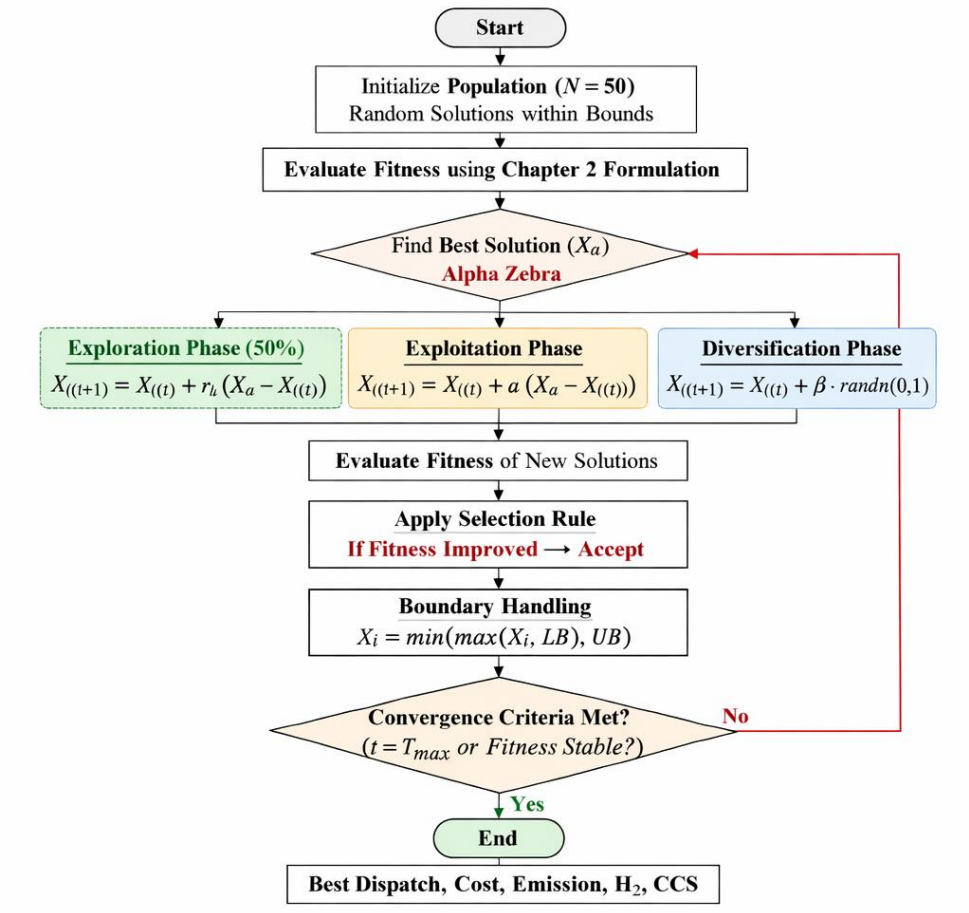

Figure 4. ZOA flowchart for DELD

Figure 4 presents the flowchart of the ZOA applied to solve the proposed multi-objective DELD problem. It outlines the initialization, exploration–exploitation–diversification phases, fitness evaluation, constraint handling, and convergence process leading to optimal dispatch, cost, emission, hydrogen, and CCS results.

3.5. Hourly Dispatch Procedure

For each hour of the 24-hour scheduling horizon:

1. Net demand is determined.
2. ZOA optimizes dispatch variables.
3. Fitness is evaluated using the formulation in Chapter 2.
4. Best hourly solution is recorded.
5. Cumulative cost and emission are computed.

3.6. ZOA Parameters Mapped to ELD Components

Table 2 provides information about ZOA parameters to the ELD parameters.

Table 2. ZOA parameters vs ELD parameters

Parameter	Symbol	Value	Role
Population Size	(N)	50	Search diversity
Maximum Iterations	Tmax	1500	Convergence depth
Exploitation Factor	α	0.1	Local refinement control
Diversification Factor	β	0.2	Avoid local minima
Penalty Weight	λ	100	Constraint enforcement

4. Results and Discussion

4.1. Case Study and Test System

The performance evaluation of the proposed integrated Dynamic Economic Emission Dispatch (DEED) framework under three operating scenarios:

- Case 1: Thermal+ PEV operation
- Case 2: Thermal + Renewable Energy Sources (RES) + PEV
- Case 3: Thermal + RES + Hydrogen Energy Storage (HES) + Carbon Capture and Storage (CCS)

The study employs a standard 10-unit thermal system widely used in DEED research for benchmarking and validation [12]. The system configuration represents a realistic medium-scale grid with renewable integration, reflecting current operational trends. A PEV fleet of 80,000 vehicles is considered to model large-scale urban electrification and its impact on system demand, consistent with prior studies [12, 14]. Vehicle characteristics, including battery capacity and SOC limits, are based on typical real-world data. Overall, the selected parameters ensure practical relevance while maintaining computational feasibility for evaluating system performance.

The nonlinear multi-objective optimization problem is solved using the Zebra Optimization Algorithm (ZOA). A ten-unit system is considered for a 24-hour scheduling horizon.

4.2. Case 1: Thermal + PEV Dispatch

In Case 1, the 24-hour load demand is supplied solely by ten thermal generating units, without renewable energy, hydrogen storage, or carbon capture integration. The dispatch minimizes fuel cost while satisfying generator limits, transmission losses, ramp-rate constraints, and power balance. System parameters, including cost coefficients, valve-point effects, emission characteristics, and loss coefficients, are adopted from [12], along with the load profile and PEV modelling. This case serves as a baseline for evaluating the impact of renewable and hydrogen-based integration.

Table 3. Comparison of ZOA and LNSGA-II for 24-Hour Dispatch under CASE 1

Method	Total Fuel Cost ($)	Total Emission (kg)
LNSGA-II [12]	24,70,741.67	2,68,421.45
ZOA	22,36,304.79	2,64,940.51

As shown in Table 3, the proposed ZOA outperforms LNSGA-II [12] under identical 24-hour load demand and PEV Scenario 4 conditions. ZOA reduces fuel cost from $2,470,741.67 to $2,236,304.79 (≈9.49% improvement) and emissions from 268,421.45 kg to 264,940.51 kg (≈1.30% reduction). This simultaneous improvement in both economic and environmental objectives demonstrates the superior convergence characteristics and solution quality of ZOA for nonlinear, multi-objective dynamic dispatch problems. These

results validate the effectiveness of the proposed methodology and highlight its advantage over the LNSGA-II approach [12].

Since no carbon capture mechanism is included in this scenario, all emissions directly contribute to the system's environmental impact. This baseline case emphasizes the importance of integrating renewable energy sources to reduce operational costs and emissions. The incorporation of wind and solar generation can decrease reliance on thermal units, mitigate valve-point nonlinearity effects, and significantly reduce fuel consumption and CO_2 emissions in power system dispatch.

4.3. Case 2: Thermal + RES + PEV Integration

Modern power systems must use renewable energy sources (RES) to reduce fuel use and carbon emissions. Variations in wind speed and solar irradiation make renewable energy generation problematic. According to[12], a 175 MW wind farm is modelled using a Weibull probability distribution with shape parameter k=1.5 and scale parameter c=15 m/s to simulate stochastic behaviour. Wind speed variation affects wind power in this probabilistic approach. Based on [12], a bimodal Weibull distribution with uncertainty weighting factor ω=0.3 is used to model a 175 MW solar PV system and simulate daily irradiance variation. Renewable power instantly balances thermal generation, and the economic dispatch model includes PV and wind operational costs.

Table 4. Comparison of Case 2 Performance Using ZOA and LNSGA-II [12]

Method	Total Fuel Cost ($)	Total Emission (kg)
LNSGA-II [12]	21,06,362.37	2,22,906.48
ZOA	20,05,181.28	2,15,129.85

Table 4 shows that the proposed ZOA outperforms LNSGA-II [12] in both economic and environmental performance under Case 2. The fuel cost is reduced from $2,106,362.37 to $2,005,181.28, resulting in a saving of $101,181.09 (≈4.80%). Similarly, total emissions decrease by 7,776.63 kg (≈3.49%), from 222,906.48 kg to 215,129.85 kg. These results indicate an improved cost – emission trade-off, demonstrating the strong convergence capability and effectiveness of ZOA for renewable-integrated dynamic dispatch problems.

In comparison with Case 1, Case 2 achieves significant improvements in both cost and emissions. The 24-hour fuel cost is reduced from $2,236,304.79 to $2,005,181.28 (≈10.34%), while emissions decrease from 264,940.51 kg to 215,129.85 kg (≈18.8%). These reductions are primarily attributed to increased renewable penetration, which reduces dependence on thermal generation.

Case 3 (Thermal + RES + Hydrogen + CCS) further extends the framework by incorporating hydrogen energy storage and carbon capture to achieve deeper emission reduction. Hydrogen enables efficient utilization of surplus renewable energy and supports temporal energy shifting, while CCS captures CO_2 emissions from thermal units, significantly reducing overall emissions with minimal impact on economic performance.

4.4. Case 3: Thermal + RES + Hydrogen + CCS

Case 3 represents the fully integrated DEED framework, incorporating wind and solar generation, PEVs, hydrogen energy storage (electrolyzer–fuel cell system), carbon capture and storage (CCS), and the benchmark 10-unit thermal system. The model simultaneously accounts for fuel cost, renewable generation cost, hydrogen system operation, emission penalties, transmission losses, and carbon capture efficiency. This scenario evaluates the techno-economic benefits of integrating hydrogen storage and CCS within a renewable-assisted DEED framework, with the objective of enhancing decarbonization and overall system performance. The corresponding system parameters for Case 3 are provided in Tables 5 and 6.

Table 5. Hydrogen Energy Storage System Parameters

Parameter	Symbol	Value	Unit	Description
Electrolyzer efficiency	η_{EL}	0.7	–	Conversion efficiency (electricity to hydrogen)
Fuel cell efficiency	η_{FC}	0.55	–	Conversion efficiency (hydrogen to electricity)
Hydrogen higher heating value	HHV_{H2}	39.4	kWh/kg	Energy content of hydrogen
Maximum electrolyzer capacity	P_{EL}^{max}	20	MW	Rated electrolyzer power
Maximum fuel cell capacity	P_{FC}^{max}	15	MW	Rated fuel cell power
Hydrogen production cost	C_{H2}^{unit}	5	per kg	Hydrogen generation cost coefficient

Table 6. Carbon Capture and Storage (CCS) Parameters

Parameter	Symbol	Value	Unit	Description
Carbon capture efficiency	η_{CCS}	0.9	–	Fraction of CO_2 captured
Energy penalty coefficient	α_{CCS}	0.00025	MW/(emission unit)	Additional power required for CCS operation
Carbon capture cost	C_{CCS}^{unit}	40	per ton	Cost of CO_2 captured

Table 7 shows that the hourly system cost in Case 3 ranges from \$68,020 (Hour 2) to \$144,100 (Hour 12), with the highest cost occurring during peak demand when thermal generation reaches 1911.6 MW and the operating costs of hydrogen systems and CCS increase. Despite these additional costs, the overall 24-hour operation remains economically viable due to the substantial reduction in emissions.

The dispatch follows economic loading principles, with reduced dependence on thermal generation compared to the baseline case. Peak thermal output is limited to 1911.6 MW, whereas it exceeds 2073.9 MW in Case 1. Base-load units operate consistently, while mid-merit units adjust their output according to renewable availability and hydrogen system operation, thereby enhancing system flexibility. Transmission losses vary from 1.7744 MW (Hour 1) to 6.9706 MW (Hour 12) and are lower than in the thermal-only case due to reduced overall generation.

Table 7. Hourly Optimal Dispatch Results of Integrated Thermal–RES–Hydrogen–CCS System

Hour	Cost ($)	Pg1 (MW)	Pg2 (MW)	Pg3 (MW)	Pg4 (MW)	Pg5 (MW)	Pg6 (MW)	Pg7 (MW)	Pg8 (MW)	Pg9 (MW)	Pg10 (MW)	PL (MW)	Emission (kg)	PT (MW)	P_EL (MW)	P_FC (MW)	H2 (kg)	CO2 Capture (kg)
1	69605	151.0	185.2	181.3	126.9	100.7	64.2	73.4	55.0	30.9	17.6	1.8	6904.1	986.1	14.7	5.4	0.0	4235.5
2	68020	150.9	223.9	87.2	119.1	203.4	111.3	77.3	77.6	28.4	12.6	2.2	598.4	1091.5	17.8	6.1	0.0	4538.2
3	72890	150.7	149.5	235.1	163.1	185.5	118.7	56.3	84.1	58.9	34.7	2.7	778.3	1236.6	11.4	4.0	0.0	5801.9
4	70423	150.1	152.0	168.0	137.0	174.3	138.4	85.6	105.0	51.0	33.3	2.5	575.4	1194.6	10.8	1.9	0.1	4674.9
5	75656	150.2	162.7	206.5	213.6	152.6	131.8	64.1	100.0	54.6	38.1	2.8	755.4	1274.1	15.7	5.0	0.0	5990.7
6	90198	150.7	243.6	300.8	157.7	218.4	147.3	114.7	100.9	43.2	31.4	4.0	1096.7	1508.7	13.7	5.0	0.0	8884.8
7	93499	177.5	230.1	267.6	245.6	233.8	125.7	57.4	101.9	56.3	40.6	4.2	2332.4	1536.4	13.3	2.9	0.1	9287.6
8	90402	150.5	198.2	333.9	243.0	167.0	148.5	97.9	99.0	51.4	39.7	4.1	1480.3	1529.1	12.2	4.2	0.0	10154
9	102810	228.9	231.8	319.4	235.2	228.7	133.1	63.8	102.8	70.0	41.4	4.9	2850.7	1654.9	19.0	5.8	0.1	11012
10	131670	326.4	395.5	254.2	259.6	212.6	124.0	99.4	116.3	73.0	32.0	6.6	2906.6	1893.0	11.5	4.1	0.0	15559
11	125050	305.4	355.2	277.2	282.9	210.8	135.1	102.4	81.2	50.5	31.5	6.2	3196.9	1832.1	16.7	4.7	0.1	14319
12	144100	469.4	302.0	317.6	207.5	225.2	126.0	79.6	90.7	50.5	43.2	7.0	5818.4	1911.6	9.7	3.7	0.0	23082
13	117020	265.9	335.4	316.4	273.4	165.4	140.0	91.4	87.7	30.3	43.7	5.6	3130.0	1749.5	17.2	4.6	0.1	13496
14	116040	302.6	301.5	326.6	239.1	221.3	127.3	86.1	89.6	37.9	23.7	5.6	2441.5	1755.8	8.4	2.6	0.0	13384
15	91429	150.1	277.8	269.5	243.0	138.5	107.6	102.3	100.6	46.0	38.6	3.9	1010.6	1474.0	14.4	4.9	0.0	8993.8
16	87287	150.1	209.8	261.7	254.5	224.7	97.6	92.5	77.2	63.9	37.1	3.8	1047.0	1469.1	18.2	6.8	0.0	8721.2
17	77255	150.7	178.0	241.5	186.7	216.6	87.4	58.0	94.3	52.2	22.8	2.9	857.8	1288.2	16.9	6.1	0.0	6682.5
18	89923	150.8	222.7	294.0	265.0	229.4	128.0	74.8	86.0	41.9	23.9	4.1	1388.9	1516.4	9.9	3.6	0.0	10004
19	94748	174.9	238.1	277.4	252.4	208.3	114.1	121.1	103.9	50.7	19.1	4.3	2218.1	1559.8	12.2	3.5	0.1	9689.5
20	129110	364.0	334.8	224.7	284.7	224.8	146.9	81.1	89.3	70.4	30.2	6.4	2843.8	1850.9	12.3	3.9	0.0	14435
21	143110	460.2	339.5	290.2	253.7	178.4	91.5	103.0	111.1	36.6	42.0	7.0	3838.3	1906.1	11.2	3.5	0.0	22138
22	96647	150.4	292.0	296.7	269.7	218.2	110.8	94.0	60.7	41.7	42.0	4.5	1459.3	1576.2	13.0	4.0	0.0	10968
23	68142	150.5	160.1	192.2	149.2	118.0	127.5	53.5	85.8	56.4	40.6	2.3	560.3	1133.8	11.4	3.0	0.1	4628.4
24	72220	150.5	190.8	158.1	184.5	171.4	106.0	93.1	83.4	50.1	18.1	2.6	689.9	1205.9	14.6	4.5	0.1	5196.6

Hydrogen energy storage plays a crucial role in stabilizing system operation. The electrolyzer power (P_{EL}) ranges from 8.40 MW to 19.03 MW, indicating active hydrogen production during periods of excess renewable generation. The fuel cell output (P_{FC}) varies between 1.86 MW and 6.83 MW, supplying electricity during peak demand conditions. Hydrogen storage levels increase during renewable-rich periods, such as Hours 4, 7, 11, and 13, demonstrating effective temporal energy shifting and improved renewable utilization.

A major advantage of Case 3 is the significant reduction in emissions. Net emissions are substantially lower than in previous cases. For instance, at Hour 12, despite high thermal generation, net emissions are limited to 5818.4 kg, while 23,082 kg of CO_2 is captured, reflecting effective carbon removal at 90% CCS efficiency. During other peak periods, carbon capture reaches 22,138 kg (Hour 21) and 15,559 kg (Hour 10), further confirming the effectiveness of CCS integration. Overall, net emissions are reduced by approximately 70–80% during high-load periods compared to Case 1, where emissions exceed 19,000 kg. This demonstrates a well-balanced techno-economic trade-off, achieving substantial emission reduction without a disproportionate increase in cost.

As shown in Table 8, the combined integration of renewable energy, hydrogen storage, and carbon capture enhances overall system sustainability. The hydrogen subsystem mitigates renewable intermittency, reduces stress on thermal units, and supports load balancing, while CCS significantly lowers carbon emissions. Although hydrogen production and CO_2 capture introduce additional costs compared to Case 2, the resulting environmental benefits and long-term decarbonization potential outweigh these increases. The integrated framework thus demonstrates strong scalability and practical applicability for future low-carbon power system operation.

Table 8. Comparative Performance Summary of All Cases

Parameter	Case 1(Thermal + PEV)	Case 2(Thermal + RES + PEV)	Case 3(Thermal + RES + H_2 + CCS)
Total Fuel Cost ($)	22,36,304.79	20,05,181.28	23,07,548.442
Renewable Cost ($)	0	9,707.77	9,707.77
Total System Cost ($)	22,36,304.79	20,14,889.05	23,17,256.21
Total Emission (kg)	2,64,940.51	2,15,129.85	50,778.92
Emission Reduction (%)	—	≈19%	≈80%
Peak Thermal Generation (MW)	2073.9	1939.9	1911.6
Peak Transmission Loss (MW)	7.65	6.59	6.97
Hydrogen Storage	No	No	Active
CO_2 Captured (kg)	0	0	2,45,876.15
Decarbonization Level	Low	Moderate	Very High

The comparative analysis highlights the impact of decarbonization on overall system performance. In Case 1 (Thermal + PEV), the system exhibits the highest fuel consumption and emissions, with total emissions of 264,940.51 kg and peak thermal generation of 2073.9 MW, resulting in increased transmission losses and operational stress. The ZOA-based dispatch demonstrates improved convergence stability and lower operating cost compared to LNSGA-II [12], indicating effective handling of nonlinear characteristics.

In Case 2 (Thermal + RES + PEV), the integration of wind and solar energy reduces peak thermal generation to 1939.9 MW, decreases fuel cost by 10.34%, and lowers emissions by 19%. The reduction in thermal dependence improves both economic and environmental performance. ZOA further enhances solution quality and constraint handling under renewable-integrated conditions compared to LNSGA-II [12].

In Case 3 (Thermal + RES + H_2 + CCS), the inclusion of hydrogen storage and carbon capture increases system cost due to additional operational requirements, but results in substantial emission reduction, achieving

nearly 80% lower net emissions. This configuration improves system flexibility through energy shifting and enhances renewable utilization.

Overall, Case 2 provides the best economic performance, while Case 3 delivers maximum environmental benefit, demonstrating a clear techno-economic trade-off. ZOA's constant improvement over NSLGA-II [12] in Cases 1 and 2 proves the optimization technique for scaled low-carbon power system transition is resilient and effective.

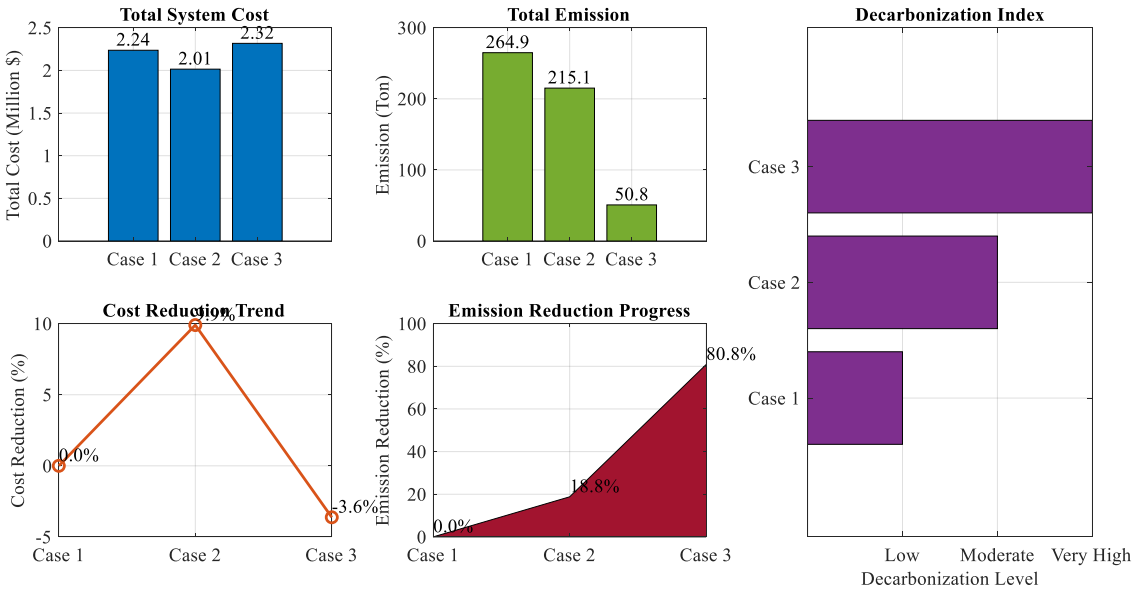

Figure 5. Techno-Economic and Emission Reduction Assessment of Thermal–RES–Hydrogen–CCS Integrated Dispatch System

Figure 5 presents a comparative techno-economic analysis of the three DEED cases. Case 2 achieves the lowest total system cost, while Case 3 provides the most significant emission reduction (≈80%) and the highest level of decarbonization. Although Case 3 results in a higher overall cost, it substantially enhances environmental performance, illustrating the trade-off between economic efficiency and deep decarbonization.

5. Conclusion

This study develops a process-integrated Dynamic Economic Emission Dispatch (DEED) framework that explicitly incorporates hydrogen energy storage and carbon capture within renewable-assisted power systems. By modelling electrolyzer–fuel cell operation through energy–mass conversion relationships and accounting for carbon capture efficiency and associated energy penalties, the framework provides a realistic representation of system behaviour compared to conventional dispatch approaches. The proposed multi-objective formulation, solved using the Zebra Optimization Algorithm (ZOA), effectively coordinates cost and emission objectives over a 24-hour horizon. Results on a standard 10-unit system show that the baseline Case 1 (Thermal + PEV) results in a total cost of $2.236 million and emissions of 264,940.51 kg. Case 2 (Thermal + RES + PEV) reduces cost by 10.34% to $2.005 million and emissions by 19% to 215,129.85 kg. Case 3 (Thermal + RES + H_2 + CCS) achieves a substantial emission reduction of approximately 80%, lowering emissions to 50,778.92 kg, while capturing 245,876 kg of CO_2, with a moderate increase in total cost to $2.317 million. The ZOA demonstrates improved convergence and superior cost–emission trade-offs compared to LNSGA-II. Overall, the integrated RES–PEV–H_2–CCS framework provides a scalable and techno-economically viable pathway for low-carbon power system operation. Future work will focus on incorporating uncertainty modelling, detailed process-level simulations, and experimental validation to further enhance practical applicability.

References

1. T. Khobaragade and K. T. Chaturvedi, “Enhanced economic load dispatch of thermal power units using TLBO algorithm,” Energies, vol. 16, no. 19, Art. no. 6933, 2023, https://doi.org/10.3390/en16196933.
2. Y. K. Reddy and M. Reddy, “Economic Load Dispatch Problem with Ant Lion Optimization Using Practical Constraints”, Gazi University Journal of Science, vol. 32, no. 2, pp. 524–542, June 2019. Available: https://izlik.org/JA62BP98FU
3. Y. Reddy and M. Reddy, “Flower pollination algorithm to solve dynamic economic loading of units with piecewise fuel options,” Indonesian Journal of Electrical Engineering and Computer Science, vol. 16, no. 1, pp. 9–16, 2019, doi: 10.11591/ijeecs.v16.i1.pp9-16.
4. J. Hetzer, D. C. Yu, and K. Bhattarai, “Economic dispatch with wind power integration,” IEEE Trans. Energy Convers., vol. 23, no. 2, pp. 603–611, 2008, doi: 10.1109/TEC.2007.914171.
5. J. Li, L. Xu, Y. Zhang, and Z. Yuan, “Economic load dispatch of integrated energy systems considering renewable uncertainty,” Processes, vol. 12, no. 8, Art. no. 1627, 2024, https://doi.org/10.3390/pr12081627.
6. Q. Meng, Y. He, and J. M. Guerrero, “Day-ahead economic dispatch of renewable-integrated microgrids,” Scientific Reports, vol. 15, Art. no. 26579, 2025, https://doi.org/10.1038/s41598-025-11561-2.
7. V., Y. Sireesha, R. Mishra, B. G., P. Badonia, S. "Grey Wolf Optimizer Algorithm for Multi-Objective Optimal Power Flow," Journal of Intelligent Systems and Internet of Things, vol. , no. , pp. 20-32, 2024. DOI: https://doi.org/10.54216/JISIoT.120102
8. B. Behera, S. Deb, and K. R. Singh, “Multi-objective dynamic dispatch with wind–solar–EV integration,” Int. J. Electr. Power Energy Syst., vol. 142, 2023, doi: 10.1016/j.ijepes.2022.108303.
9. D. Hmingthanmawia, S. Deb, and K. R. Singh, “Multi-objective economic dispatch considering electric vehicle penetration,” Frontiers in Energy Research, vol. 12, Art. no. 1389822, 2024, https://doi.org/10.3389/fenrg.2024.1389822.
10. Behera, S., Behera, S., & Barisal, A. K. (2022). Dynamic Combined Economic Emission Dispatch integrating Plug-in Electric Vehicles and Renewable Energy Sources. International Journal of Ambient Energy, 43(1), 4683–4700. https://doi.org/10.1080/01430750.2021.1918243.
11. H. Zeynal, Y. Jiazhen, B. Azzopardi and M. Eidiani, "Impact of Electric Vehicle's integration into the economic VAr dispatch algorithm," 2014 IEEE Innovative Smart Grid Technologies - Asia (ISGT ASIA), Kuala Lumpur, Malaysia, 2014, pp. 780-785, doi: 10.1109/ISGT-Asia.2014.6873892.
12. Reddy, Y., Revathi, K., Rajak, S., Manohar, C., Naidu, M., Krishna Reddy, Y. V., “Optimizing Cost and Emissions in a 10-Unit Power Generation System using Different Optimization Techniques with Wind Energy Integration,” IEEE International Conference on Distributed Computing, Electrical and Electronics Engineering (ICDCECE), 2025, pp. 1–6.
13. J. Soni and K. Bhattacharjee, “Economic emission dispatch with renewable energy and electric vehicle integration,” Indian J. Pure Appl. Phys., vol. 63, no. 10, pp. 930–944, 2025.
14. D. Zou, L. Ma, C. Li, and H. Ouyang, “Integration of the wind and solar power for the dynamic economic emission dispatch with the charging and discharging of plug-in electric vehicles,” Engineering Applications of Artificial Intelligence, vol. 138, pt. A, Art. no. 109293, 2024, doi: 10.1016/j.engappai.2024.109293.
15. S. Naresh, I. Anupalli, “Electric vehicle integration in economic load dispatch with renewable energy sources: A systematic literature review,” E3S Web of Conferences, vol. 692, Art. no. 02001, 2026, doi: 10.1051/e3sconf/202669202001.
16. H. Zhang and Y. Wang, “Stochastic economic dispatch of wind–EV coupled systems,” Energy, vol. 296, 2024, doi: 10.1016/j.energy.2024.130486.
17. A. Abdelaziz, E. Ali, and S. Abd Elazim, “Solar-assisted economic dispatch using metaheuristic optimization,” Electric Power Components and Systems, vol. 52, no. 4, pp. 345–357, 2024, doi: 10.1080/15325008.2023.2289426.
18. Sreekakulam Naresh, Immanuel Anupalli, "Dynamic Economic Load Dispatch for Grids with Hybrid Energy Systems and Plug-in EVs," SSRG International Journal of Electrical and Electronics Engineering, vol. 12, no. 11, pp. 104-111, 2025. Crossref, doi:10.14445/23488379/IJEEE-V12I11P109
19. R. Mehta and N. Gupta, “Optimal dispatch of solar-integrated power systems with EVs,” Renewable Energy, vol. 226, pp. 1200–1212, 2025, doi: 10.1016/j.renene.2024.01.082.
20. S. Jain et al., “Coordinated solar–EV economic dispatch using hybrid optimization,” Journal of Cleaner Production, vol. 418, 2024, doi: 10.1016/j.jclepro.2024.138033.
21. S. Guo, “Economic dispatch model of renewable energy systems considering demand response,” Int. J. Renewable Energy Development, vol. 14, no. 2, pp. 311–321, 2025, https://doi.org/10.61435/ijred.2025.60680.
22. Mansir IB, Okonkwo PC, Qahtan TF. A review of hydrogen production and storage technologies for power system integration and applications. Glob Energy Interconnect. 2026;9(1):83-107. doi:10.1016/j.gloei.2026.01.001.
23. Wei S, Li Q, Zheng W, Han Y, Yu Z, Bai Z, Han Y. Enhancing wind-solar hybrid hydrogen production through multi-state electrolyzer management and complementary energy optimization. Energy Rep. 2024;11:1774-1786. doi:10.1016/j.egyr.2024.01.031.

24. Wang J, Pan Z, Ge H, Zhao H, Xia T, Wang B. Economic Dispatch of Integrated Electricity–Heat–Hydrogen System Considering Hydrogen Production by Water Electrolysis. Electronics. 2023; 12(19):4166. https://doi.org/10.3390/electronics12194166.
25. Zhu Y, Niu S, Dai G, Li Y, Wang L, Jia R. Optimal Economic Dispatch of Hydrogen Storage-Based Integrated Energy System with Electricity and Heat. Sustainability. 2025; 17(5):1974. https://doi.org/10.3390/su17051974.
26. Chen Y, Dong X, Wang G, Lv D, Gu R, Lei Y. Low-carbon economic dispatch of integrated energy system with CCS-P2G-CHP. Energy Rep. 2024;12:42-51. doi:10.1016/j.egyr.2024.05.055.
27. Ding C, Zhou Y, Ding Q, Li K. Integrated Carbon-Capture-Based Low-Carbon Economic Dispatch of Power Systems Based on EEMD-LSTM-SVR Wind Power Forecasting. Energies. 2022; 15(5):1613. https://doi.org/10.3390/en15051613.
28. V. R. Birudala and C. Chinthapudi, “Solar–wind fed EV charger at variable irradiance and wind speeds,” in Proc. i-PACT, Kuala Lumpur, Malaysia, 2023, pp. 1–4, doi: 10.1109/i-PACT58649.2023.10434840.
29. B. V. Reddy and C. Chengaiah, “A modified P&O technique for solar-based EV charging with SEPIC,” in Proc. ICECCT, Erode, India, 2023, pp. 1–4, doi: 10.1109/ICECCT56650.2023.10179607.
30. B. V. Reddy and C. Chengaiah, “Simulation and analysis of solar–wind system for EV charging,” IOP Conf. Ser.: Earth Environ. Sci., vol. 1382, Art. no. 012003, 2024, doi: 10.1088/1755-1315/1382/1/012003.
31. B. V. Reddy, C. Chengaiah, and S. R. Salkuti, “Simulation and analysis of solar–wind system for EV charging,” in Energy and Environmental Aspects of Emerging Technologies for Smart Grid, Springer, Cham, 2024, doi: 10.1007/978-3-031-18389-8_7.
32. V. R. Birudala and B. J. Adinarayana, “A PV–wind based EV charging station under dynamic weather conditions,” in Proc. ICAECA, Coimbatore, India, 2025, pp. 1–6, doi: 10.1109/ICAECA63854.2025.11012316.
33. A. Faramarzi, M. Heidarinejad, and S. Mirjalili, “Zebra optimization algorithm: A new nature-inspired metaheuristic for solving optimization problems,” Applied Soft Computing, vol. 131, 2022, doi: 10.1016/j.asoc.2022.109622.